Published in *Materials Letters*, 151, 2015, pp126-129. doi:10.1016/j.matlet.2015.03.066

Hardening of an $Al_{0.3}CoCrFeNi$ high entropy alloy via high-pressure torsion and thermal annealing

Q.H. Tang [a], Y. Huang [b], Y.Y. Huang [c], X.Z. Liao [d,*], T.G. Langdon [b,e], and P.Q. Dai [a,c,*]

[a] College of Materials Science and Engineering, Fuzhou University, Fuzhou 350108, China

[b] Materials Research Group, Faculty of Engineering and the Environment, University of Southampton, Southampton SO17 1 BJ, UK.

[c] School of Materials Science and Engineering, Fujian University of Technology, Fuzhou 350108, China

[d] School of Aerospace, Mechanical and Mechatronic Engineering, The University of Sydney, Sydney, NSW 2006, Australia

[e] Departments of Aerospace & Mechanical Engineering and Materials Science, University of Southern California, Los Angeles, CA 90089-1453, USA

Abstract

High-pressure torsion (HPT) and thermal annealing were applied to a face-centered cubic as-cast $Al_{0.3}CoCrFeNi$ high entropy alloy. Processing by HPT produced a nanostructure with a higher incremental hardness than in most HPT single-phase materials and subsequent annealing at appropriate temperatures gave an ordered body-centered cubic secondary phase with an additional increase in hardness. The highest hardness after HPT and annealing was approximately four times higher than for the as-cast alloy.

Keywords: High entropy alloy; High-pressure torsion; Annealing; Hardening

[*] Corresponding authors: Tel: 61 2 9351 2348; Fax: 61 2 9351; 7060; E-mail address: xiaozhou.liao@sydney.edu.au (X.Z. Liao), Tel: +86 591 22863280; fax: +86 591 22863279; E-mail address: pqdai@126.com (P.Q. Dai)

Published in *Materials Letters*, 151, 2015, pp126-129. doi:10.1016/j.matlet.2015.03.066

1. Introduction

High entropy alloys (HEAs) contain five or more principal elements with each elemental concentration between 5 at.% and 35 at.% [1] and the materials are attractive because of their unusual structural properties [2-9]. While extensive efforts have been made to explore the effects of alloying on the phases, phase transformations during thermal processing and the mechanical and corrosion properties of coarse-grained (CG) HEAs [2-6], there are only a few reports describing the influence of ultrafine grains on the mechanical properties and thermal stability [7-9].

Refining grains to the submicrometer or even the nanometer scale may lead to superior properties including a combination of high strength and reasonably good ductility [10, 11]. Severe plastic deformation (SPD) is an efficient way to fabricate bulk ultrafine-grained (UFG) and nanocrystalline (NC) materials [12-15] and processing by high-pressure torsion (HPT) is especially effective because it can impose an exceptionally high strain [16]. Using a thermal treatment to form secondary phases (for example, fine precipitates) is another important method for achieving strengthening [17, 18]. In practice, the inherent sluggish diffusion effect in CG HEAs hampers the growth of secondary phases during thermal treatment and this leads to high densities of fine grains of the secondary phases that strengthen the HEAs [1, 2, 19]. Thus, it appears that a combination of HPT and thermal treatment may significantly improve the strength of HEAs and make these alloys more attractive for many structural applications.

To investigate this possibility, the present research was initiated to investigate HPT

processing and thermal treatment of an $Al_{0.3}CoCrFeNi$ (atomic ratio) HEA having a face-centered cubic (FCC) structure. The alloy was processed by HPT at room temperature and then subjected to thermal annealing at various elevated temperatures. The resulting high values of hardness and the mechanism of microstructural evolution are examined in this report.

2. Experimental material and procedures

The $Al_{0.3}CoCrFeNi$ HEA was prepared by vacuum induction melting of the constituent elements having at least 99.9 wt.% purity. The alloy was melted five times to improve its chemical homogeneity. The as-cast alloy was machined into discs with a diameter of 10 mm and a thickness of ~0.8 mm for HPT processing. The processing was performed at room temperature using a quasi-constrained HPT facility [20] under an applied pressure of 6.0 GPa and a rotation rate of 1 rpm for 8 revolutions in order to achieve a steady-state grain size and a reasonably homogenous microstructure. This HPT HEA is henceforth designated NC-RT denoting nanocrystalline at room temperature.

Specimens with diameters of 3 mm were cut from the edges of the HPT discs for further thermal processing. Thermal annealing was carried out at temperatures of 573, 673, 773, 873 and 973 K for 1 h; these HEA samples are referred to as NC-573, NC-673, NC-773, NC-873 and NC-973, respectively. For comparison, the CG as-cast samples were also annealed at these temperatures.

The hardness was measured using a DHV-1000 Vickers microhardness tester with an applied load of 200 g and a dwell time of 15 s. The reported values are the average of at

least seven datum points. X-ray diffraction (XRD) was conducted using a Bruker D8 Advance diffractometer equipped with a Cu target. The dislocation density, ρ, was estimated from the XRD patterns using the relationship [21,22] $\rho = \frac{2\sqrt{3}<\varepsilon^2>^{1/2}}{db}$, where d is crystallite size, $<\varepsilon^2>^{1/2}$ is microstrain, and b is the absolute value of the Burgers vector of $\frac{1}{2}<110>$ for FCC metals. The errors for the dislocation density and lattice parameter measurements, as assessed by scanning each specimen three times, were less than 10% and 0.0005 nm, respectively. Transmission electron microscopy (TEM) observations were performed using a JEM-2100 microscope operating at 200 kV. The average grain sizes were statistically estimated by measuring at least 200 grains along two orthogonal axes from the TEM images.

3. Results and discussion

Figure 1 shows the Vickers hardness of the as-cast and HPT HEA before and after annealing at different temperatures. The as-cast HEA, having a typical CG structure with grain sizes ranging from ~100 to ~1100 μm (average ~350 μm), had a hardness of ~150. After HPT, the hardness increased to ~530. This incremental increase in hardness of ~380 converts to an increase of ~3.7 GPa which is higher than the HPT-induced hardness increments of most single-phase materials where the increases are generally lower than ~3.1 GPa: a summary of these numbers is given by Edalati et al. [23]. For conventional single-phase alloy systems, introducing solute atoms can enhance solid-solution hardening and produce greater grain refinement compared to pure metals [23]. Since all

principal elements acting as solute atoms were introduced to HEAs [1, 2], it is reasonable to anticipate that HEAs should have a strong potential for strengthening via SPD. This is readily proven by the experimental data in Fig. 1.

Annealing at different temperatures showed different effects on the Vickers hardness of the HPT HEA. Therefore, the annealing temperature range was divided into three regions as shown in Fig. 1. Annealing up to 573 K in region I produces no change in hardness but increasing the annealing temperature to 773 K in region II leads to increased hardness and a peak value of ~615 which is about 4 times higher than the hardness of the as-cast HEA. Further increasing the annealing temperature to region III reduces the hardness monotonously. The results demonstrate that a combination of HPT and annealing at appropriate temperatures is an effective method for improving the strength of HEAs. By comparison, the effect of annealing on the hardness of the as-cast HEA is also presented in Fig.1. Generally, the results for the as-cast CG material show a similar trend but the hardness starts to increase at a higher temperature of about 773 K.

Figure 2 shows XRD patterns of HPT HEA before and after annealing at different temperatures. Only the single FCC phase was detected when annealing at or below 573 K. At 673 and 773 K, new peaks appear at $2\theta \approx 30°$ and $2\theta \approx 45°$ and they are identified as 100 and 110 diffraction of the ordered body-centered cubic (BCC) phase in the alloy [4]. The 100 peak reaches its highest intensity at 773 K suggesting an increase in the amount of the BCC phase at least until 773 K. The 100 peak disappears at higher temperatures and this is probably caused by the variation of preferred orientation of the ordered BCC phase because the 110 peak remains and selected-area electron diffraction (SAED)

patterns (see Fig. 3) confirm the ordered BCC phase at higher temperatures. The XRD data suggest the coexistence of two phases after annealing at or above 673 K.

Figure 3 shows the microstructure of the HPT HEA after annealing in different temperature regions. In region I, nanoscale equiaxed grains with ill-defined grain boundaries (GBs) were observed (Fig. 3a). This type of GB structures is very similar to earlier reports of other SPD materials and it is due to the presence of non-equilibrium GB configurations with the presence of non-geometrically necessary dislocations at the GBs [13, 24, 25]. In region II, the GBs became sharp and well-defined (Fig. 3b). This change in GB morphology is associated with dislocation annihilation. Figure 3c shows the formation of a secondary phase preferentially in the vicinity of the matrix GBs. A Fourier transformation of a high-resolution TEM image of the secondary phase in Fig. 3c confirms that the secondary phase is the ordered BCC phase. In region III, grain growth clearly occurs for both the matrix and the secondary phase (see Fig. 3d and Table 1) and the SAED patterns (insets in Fig. 3d) confirm the co-existence of the FCC matrix and the ordered BCC secondary phase. An electron energy dispersive spectroscopy analysis (results shown in Fig. 3d) reveals that the secondary phase contains significantly more Al and Ni than in the matrix. A similar Al- and Ni-rich ordered BCC phase was reported in other CG Al-contained HEA systems [5, 18] and the ordered BCC phase is more brittle and stronger than the FCC matrix [4, 5].

Table 1 lists the dislocation densities and lattice parameters obtained from the XRD analysis and average grain sizes from the TEM measurements. The dislocation density decreases monotonously with increasing annealing temperature and this is responsible for

the formation of well-defined GBs in region II. The evolution of lattice parameters reflects the change in the compositions of the two phases. At or below 573 K, the lattice parameter of the FCC phase remains almost constant indicating an absence of elemental diffusion. At 673 K and above, the lattice parameter of the FCC phase first decreases and then stabilizes while that of the ordered BCC phase shows an opposite trend. These lattice parameter evolutions are due to a partitioning of Al from the FCC phase to the ordered BCC phase. No major grain growth is observed in region I but there is a minor increase in the grain sizes of the two phases in region II and very significant growth in region III. The average grain sizes of the FCC and the ordered BCC phases at 973 K are ~7 and ~6 times larger than those at 773 K, respectively.

The results show that grain refinement plays an most important role for the hardness increment since it contributes ~82% of the increment after HPT and annealing at 773 K. The contribution of the dislocation density to the hardness is almost negligible for the nanocrystalline alloy since a reduction of ~42% in the dislocation density after annealing at 573 K gave no significant change in the hardness. The formation of the hard secondary order BCC phase contributes about 18% of the total hardness increment at 773 K. The slight increase in grain size at this temperature appears to have only a minor effect on the hardness. As annealing temperature further increases above 773 K, the significant grain growth in both the FCC and the ordered BCC phases becomes more predominantly responsible for an overall hardness reduction because of the Hall-Petch effect [26, 27].

4. Summary and conclusions

The results demonstrate that a combination of HPT processing and thermal annealing significantly strengthens the hardness of an $Al_{0.3}$CoCrFeNi HEA. The highest hardness achieved is approximately 4 times larger than the original hardness of the as-cast HEA. Mechanical testing and structural characterization shows that most of this incremental increase in hardness is due to grain refinement to the nanometer range. The formation of a hard secondary phase during thermal annealing, where this is Al- and Ni-rich and of an ordered BCC structure, further increases the hardness. Nevertheless, annealing at very high temperatures gives grain growth in both the matrix and the secondary phase and this reduces the overall hardness.

Acknowledgements

QHT and PQD appreciate the scientific fund of the Fujian University of Technology (Grant No. E0600133). XZL thanks the Australian Research Council for financial support. This work was supported in part by the European Research Council under ERC Grant Agreement No. 267464-SPDMETALS (YH and TGL).

Published in *Materials Letters*, 151, 2015, pp126-129. doi:10.1016/j.matlet.2015.03.066

References

[1] Yeh JW, Chen SK, Lin SJ, Gan JY, Chin TS, Shun TT, et al. Adv Eng Mater 2004; 6: 299–303.

[2] Zhang Y, Zuo TT, Tang Z, Gao MC, Dahmen KA, Liaw PK. Prog Mater Sci 2014; 61: 1-93.

[3] Otto F, Dlouhý A, Somsen Ch, Bei H, Eggeler G, George EP. Acta Mater 2013; 61: 5743–5755.

[4] He JY, Liu WH, Wang H, Wu Y, Liu XJ, Nieh TG, et al. Acta Mater 2014; 62: 105–113.

[5] Kao YF, Chen TJ, Chen SK, Yeh JW. J Alloys Compd 2009; 488: 57–64.

[6] Chou YL, Yeh JW, Shih HC. Corros Sci 2010; 52: 2571-2581.

[7] Romankov S, Park YC, Shchetinin IV, Yoon JM. Acta Mater 2013; 61: 1254-1265.

[8] Chen WP, Fu ZQ, Fang SC, Wang YP, Xiao HQ, Zhu DZ. Mater Sci Eng A 2013; 565: 439-444.

[9] Varalakshmi S, Kamaraj M, Murty BS. Mater Sci Eng A 2010; 527: 1027-1030.

[10] Valiev RZ, Islamgaliev RK, Alexandrov IV. Prog Mater Sci 2000; 45: 103-189.

[11] Meyers MA, Mishra A, Benson DJ. Prog Mater Sci 2006; 51: 427–556.

[12] Zhao YH, Liao XZ, Cheng S, Ma E, Zhu YT. Adv Mater 2006; 18: 2280–3.

[13] Zhao YH, Liao XZ, Jin Z, Valiev RZ, Zhu YT. Acta Mater 2004; 52: 4589–4599.

[14] Valiev RZ, Langdon TG. Prog Mater Sci 2006; 21: 881-981.

[15] Langdon TG. Acta Mater 2013; 61: 7035-7059.

[16] Zhilyaev AP, Langdon TG. Prog Mater Sci 2008; 53: 893–979.

[17] Shun TT, Du YC. J Alloys Compd 2009; 479: 157–160.

[18] Chen ST, Tang WY, Kuo YF, Chen SY, Tsau CH, Shun TT, et al. Mater Sci Eng A 2010; 527: 5818–5825.

[19] Tsai KY, Tsai MH, Yeh JW. Acta Mater 2013; 61: 4887–4897.

[20] Figueiredo RB, Cetlin PR, Langdon TG. Mater Sci Eng A 2011; 528: 8198-8204.

[21] Williamson GK, Smallman RE. Philos Mag 1956; 1: 34–6.

[22] Smallman RE, Westmacott KH. Philos Mag 1957; 2: 669–683.

[23] Edalati K, Akama D, Nishio A, Lee S, Yonenaga Y, Cubero-Sesin JM, et al. Acta Mater 2014; 69: 68–77.

[24] Horita Z, Smith DJ, Furukawa M, Nemoto M, Valiev RZ, Langdon TG. J Mater Res 1996; 11: 1880–1890.

[25] Wang YB, Liao XZ, Zhao YH, Lavernia EJ, Ringer SP, Horita Z, et al. Mater Sci Eng A 2010; 527: 4959–4966.

[26] Hall EO. Proc Phys Soc B 1951; 64: 747–753.

[27] Petch NJ. J Iron Steel Inst 1953; 174: 25–8.

Published in *Materials Letters*, 151, 2015, pp126-129. doi:10.1016/j.matlet.2015.03.066

Figure captions

Fig. 1 The dependence of Vickers hardness of the as-cast and HPT HEA on the annealing temperature.

Fig. 2 XRD patterns of the HPT HEA before and after annealing.

Fig. 3 TEM images taken from: (a) a NC-RT sample; (b) a NC-773 sample; (c) a high-resolution image also from a NC-773 sample. A white square in (c) indicates an area where secondary phase formed, as evidenced by the Fourier transformation of the area at the top-left inset; (d) a NC-973 sample. Two circles in (d) indicate the places where electron energy dispersive spectroscopy data and SAED patterns were obtained. <011> SAED patterns from the matrix and the secondary phase were presented at the top-left and top-right insets, respectively.

Published in *Materials Letters*, 151, 2015, pp126-129. doi:10.1016/j.matlet.2015.03.066

Table 1 The calculated dislocation density (ρ) in the FCC matrix, the lattice parameters of the FCC and ordered BCC phases (a_{FCC} and a_{BCC}), and the TEM observed average grain sizes (d_{FCC} and d_{BCC}) of the HPT HEAs before and after annealing at different temperatures.

Samples	Region I		Region II		Region III	
	NC-RT	NC-573	NC-673	NC-773	NC-873	NC-973
ρ (m^{-2})	1.1×10^{15}	6.4×10^{14}	3.8×10^{14}	7×10^{13}	3×10^{13}	1×10^{13}
a_{FCC} (nm)	0.3595	0.3596	0.3593	0.3583	0.3579	0.3580
a_{BCC} (nm)	-	-	0.2836	0.2844	0.2870	0.2871
d_{FCC} (nm)	30	30	33	40	90	280
d_{BCC} (nm)	-	-	8	10	30	60

Figure 1

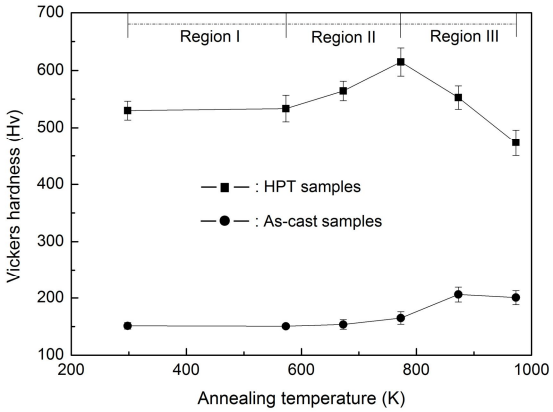

Figure 2

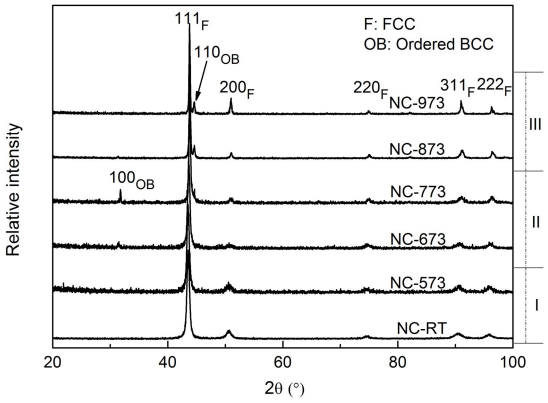

Figure 3